Physics of the Earth and Planetary Interiors 363 (2025) 107352

Contents lists available at ScienceDirect

Physics of the Earth and Planetary Interiors

journal homepage: www.elsevier.com/locate/pepi

The history of geomagnetic secular variation hemispherical dichotomies

Mathis Colas, Filipe Terra-Nova *, Hagay Amit

Nantes Université, Univ Angers, Le Mans Université, Laboratoire de Planétologie et Géosciences, CNRS UMR 6112, 2 rue de la Houssinière, F-44000 Nantes, France

ARTICLE INFO

Keywords:
Magnetic field
Secular variation
Archeomagnetic field
Paleomagnetic field
Pacific-Atlantic dichotomy

ABSTRACT

Monitoring the geomagnetic field and its secular variation (SV) is essential for understanding the Earth's internal dynamics. In particular, the SV provides an image of the geodynamo at the top of the core. However, the SV is not available for paleomagnetic field models. Here, we propose a new index for assessing the paleomagnetic SV. This new index is based on the well-established inverse linear relationship between the SV timescales and the degree of spherical harmonics. We demonstrate using the historical field where the SV is available that this index adequately captures the large-scale features of the true SV, in particular the SV Atlantic/Pacific and North/South dichotomies. The recovery of these SV hemispherical dichotomies by our proposed index does not deteriorate from truncated fields at spherical harmonics degree 14 to 5. Applied to a paleomagnetic field model for the past 100 kyr, we find a persistent SV dichotomy between the quiet Pacific and active Atlantic hemispheres, consistent with heterogeneous inner core freezing. In addition, according to our index, a persistent stronger SV prevails at the northern hemisphere, which is the case at the present day due to a fast westward jet at high latitudes of the northern hemisphere.

1. Introduction

The geomagnetic field is sustained by fluid dynamics in the Earth's liquid metallic outer core, a process termed “geodynamo”. Temporal variations in the Earth's magnetic field (the so-called secular variation (SV)) result from the transport of the field by the flow within the outer core and its decay by magnetic diffusion (e.g. Backus et al., 1996). The current geomagnetic field is monitored by surface observatories and dedicated satellites, providing direct measurements which are used to produce high-resolution models of the field and its SV expanded until spherical harmonic degree and order 14 (Sabaka et al., 2020; Finlay et al., 2020; Huder et al., 2020). Studying and understanding the phenomena that induce the geomagnetic field and its SV at the core-mantle boundary (CMB) is of great importance, because it provides crucial information about core dynamics. In particular, it allows to invert for the flow at the top of the Earth's outer core (Holme, 2015; Finlay et al., 2023).

The spatial distribution of the geomagnetic SV may provide insight into the dynamics below the CMB. Historical geomagnetic field models show a dichotomy in the SV between the Atlantic and Pacific hemispheres (Bloxham and Gubbins, 1985; Holme et al., 2011). Hulot et al. (2002) showed using geomagnetic data from the Oersted and Magsat satellites from 1980 to 2000 that the SV is much stronger in the Atlantic hemisphere than in the Pacific hemisphere. Several mechanisms to explain the Pacific/Atlantic SV dichotomy have been proposed. Christensen and Olson (2003) found in a dynamo simulation with outer boundary heat flux heterogeneity inferred from a lower mantle seismic tomography model strong westward drift below the Atlantic as opposed to eastward drift below east Pacific. Motivated by observed seismic anomalies at the top of the inner core (Tanaka and Hamaguchi, 1997), Aubert et al. (2013) demonstrated using a numerical dynamo simulation that the Pacific/Atlantic SV dichotomy may be caused by heterogeneous freezing and growth of the Earth's inner core, which leads to preferential morphology of the flow in the outer core and a concentration of SV under the Atlantic hemisphere. Alternatively, Dumberry and More (2020) explained the Pacific/Atlantic SV dichotomy by heterogeneous electrical conductivity in the lower mantle. If the conductance of the lower mantle is larger below the Pacific, the core flow would be deflected away from the Pacific hence weaker SV would be induced there. However, there is no seismic evidence for such distribution of lower mantle conductance (Dumberry and More, 2020).

In addition to longitudinal hemispherical dichotomy, at present the SV is significantly larger in the northern hemisphere than in the southern (see polar projections in Fig. 1b). Livermore et al. (2017) argued that the strong geomagnetic SV in northern high latitudes is caused by a strong westward jet there. On short timescales (decades to centuries),

* Corresponding author.
E-mail address: filipe.terranova@univ-nantes.fr (F. Terra-Nova).

https://doi.org/10.1016/j.pepi.2025.107352
Received 17 December 2024; Received in revised form 28 March 2025; Accepted 8 April 2025
Available online 11 April 2025

dominant effects of rapid rotation are expected to give a high level of equatorial symmetry in the core flow (e.g. Busse, 1970; Jault, 2008), so the strong jet located at high latitudes of the northern hemisphere should also be present in the same latitudes of the southern hemisphere. However, no strong SV is observed at high latitudes of the southern hemisphere (see South polar projection in Fig. 1b).

Prior to direct measurements (Gauss, 1833), the data available for constructing geomagnetic field models originates from geological or archaeological objects bearing a natural remanent magnetization (e.g. Tauxe, 2010). These observations are very uncertain and scattered in time and space. In particular, the data becomes gradually less abundant with increasing age. For example, over the last 100 kyr the data density drops markedly prior to the year −60,000 (Panovska et al., 2018b). Consequently, archeo- and paleomagnetic field models have larger knot point spacing of the splines compared to historical geomagnetic field models (e.g. Korte et al., 2009). In particular, the low temporal resolution leads to time-dependent global spherical harmonic paleomagnetic field models that lack SV Gauss coefficients (e.g. Panovska et al., 2018b; Nilsson et al., 2022). Ancient global field models rely on grouping data per bins of decades to centuries which acts effectively as a temporal regularization (Korte et al., 2009; Sanchez et al., 2016; Panovska et al., 2018b; Nilsson et al., 2022). Taking into account that the outer core advection time is about 140 yr (Terra-Nova and Amit, 2020) and the SV timescales associated with small-scale field are even shorter (e.g. Lhuillier et al., 2011; Amit et al., 2018), it renders the construction of global SV paleo- and archaeomagnetic Gauss coefficients unfeasible.

To overcome this problem, a paleo SV index, denoted P_i, that measures the deviation of the surface field from its main component (the axial dipole) was proposed by Constable et al. (2016). Using paleomagnetic field models of the past 10 kyr and of the past 100 kyr, persistent large P_i was found in the southern hemisphere (Constable et al., 2016; Panovska et al., 2018b). In addition, Constable et al. (2016) also reported large P_i temporal variability in the southern hemisphere. Panovska and Constable (2017) demonstrated that high paleo SV index events correlate well with the occurrence of reversals and excursions. Following studies thus used P_i to successfully identify reversals and excursions (Korte et al., 2019; Mahgoub et al., 2024; Mason et al., 2024). Mound and Davies (2023) applied this paleo SV index to the 100 kyr paleomagnetic field model of Panovska et al. (2018b). They argued that the Pacific/Atlantic SV dichotomy based on P_i is weak, concluding that the longitudinal SV hemispherical dichotomy is a recent phenomenon rather than a persistent feature of the geodynamo. Mound and Davies (2023) therefore ruled out the hypothesis that the geodynamo is controlled by a heterogeneous inner core growth (Aubert et al., 2013). However, Virtual Geomagnetic Poles scatter (e.g. Biggin et al., 2008) inferred from paleomagnetic data from Saint Helena and Trindade island combined with a selected data set reveal a 23 % stronger scatter in the Atlantic than in the Pacific hemisphere for the past 10 Myr (Engbers et al., 2020; de Oliveira et al., 2024).

In this study, we propose an alternative index to estimate the paleomagnetic SV, based on the timescales of geomagnetic SV. These timescales are defined by the ratio between the power spectra of the field and the SV (Hulot and Le Mouël, 1994), corresponding to the time needed for a field of a given spherical harmonic degree to get reorganized so that it is no longer correlated with its previous state (Stacey and Davis, 2008). Previous studies reported an inverse linear relationship between the non-dipole SV timescales and the degree of spherical harmonics (Christensen and Tilgner, 2004; Lhuillier et al., 2011; Bouligand et al., 2016; Amit et al., 2018; Tsang and Jones, 2024). It is on the basis of this inverse linear relationship that our new index is formulated.

We first use a state of the art historical geomagnetic field model based on surface observatories and satellite data to compare our new index and the PSV index of Constable et al. (2016) to the true SV density. We then apply the two indices to paleomagnetic field models in order to characterize the SV at the top of the core in the far past. Large-scale historical SV features, such as the Pacific/Atlantic and North/South hemispherical SV dichotomies, are investigated to determine whether these features are persistent or transient.

Our analysis relies on the validity of global ancient field models. Obviously, biases in paleomagnetic field models due to low data density in space and time (Cromwell et al., 2018) might lead to false interpretations. The data is more sparse in the southern hemisphere and oceans (Panovska et al., 2018a). Consequently, global paleomagnetic field models are expanded to a lower degree of spherical harmonics than historical field models (Panovska et al., 2018b). Newly acquired paleomagnetic data (e.g. Nowaczyk et al., 2025) is essential in order to produce more robust field models which may provide better insight into persistent large-scale properties of the geomagnetic SV.

The paper is organized as follows. In Section 2, the two PSV indices (old and new) are presented and measures of hemispherical dichotomies are defined. The results obtained from both indices are presented in Section 3 and discussed in Section 4.

2. Methods

2.1. Paleomagnetic secular variation index

The first index used in this study to investigate the spatial pattern of the secular variation (SV) was proposed by Constable et al. (2016). The Paleomagnetic Secular Variation Index (PSV index or P_i) measures the

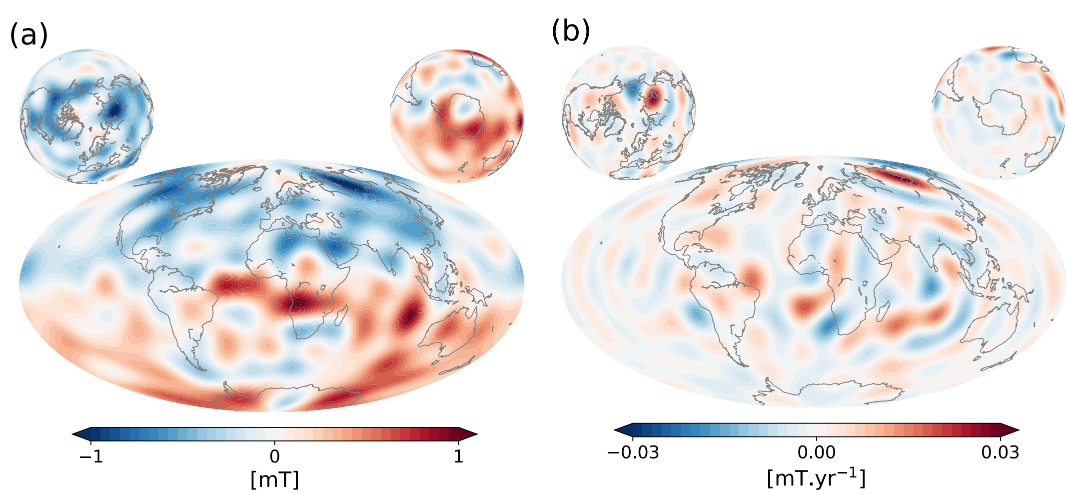

Fig. 1. The radial component of the geomagnetic field (a) and its SV (b) at the CMB for the year 2010 based on the mean of the ensemble model COV-OBS.x2 (Huder et al., 2020).

deviation of the field at a point on the surface of the globe from a geocentric axial dipole. To calculate P_i, the three components of the surface magnetic field, the intensity F, inclination I and declination D are used. These three components are defined by

$$F = \sqrt{B_\phi^2 + B_\theta^2 + B_r^2} \tag{1}$$

$$I = \arcsin\left(\frac{-B_r}{F}\right) \tag{2}$$

$$D = \arctan\left(\frac{-B_\phi}{B_\theta}\right) \tag{3}$$

where B_ϕ, B_θ and B_r are the magnetic field components in the longitude, co-latitude and radial directions. Fig. 2 shows F, I and D spatial distributions in 2010.

The index P_i is defined as follows

$$P_i(\lambda, \phi, t) = \frac{(\pi/2 - |\lambda_p(\lambda, \phi, t)|)M_0}{\pi M(\lambda, \phi, t)} \tag{4}$$

where λ and ϕ are the geographical coordinates (latitude and longitude), M_0 the historical dipole moment magnitude $M_0 \approx 8{\cdot}10^{22}$ Am^2 (Olson and Amit, 2006), λ_p the latitude of the magnetic pole

$$\lambda_p = \sin^{-1}(\sin\lambda\cos p + \cos\lambda\sin p\cos D) \tag{5}$$

and the virtual dipole moment is

$$M = \frac{4\pi a^3}{\mu_0}\frac{F}{\sqrt{1 + 3\cos^2 p}} \tag{6}$$

where a is the average value of the Earth's radius and μ_0 the permeability of free space. The magnetic co-latitude p in (5) and (6) is calculated using the dipole formula (Butler, 1992) as

$$p = \tan^{-1}\left(\frac{2}{\tan\ I}\right). \tag{7}$$

2.2. A new index for the geomagnetic secular variation

Our objective is to explain large-scale SV features on the CMB. Because only the radial field is continuous across the CMB, only this component is commonly used to infer core dynamics (e.g. Bloxham and Jackson, 1991; Holme, 2015; Finlay et al., 2023). Therefore, we define our alternative index based on the radial field on the CMB.

The second index, which we term T_i, is derived based on the concept of the SV timescales. The degree-dependent SV timescales (Hulot and Le Mouël, 1994) are defined by the power spectra R_ℓ and S_ℓ

$$\tau_\ell = \sqrt{\frac{R_\ell}{S_\ell}} \tag{8}$$

where R_ℓ is the power spectrum of the magnetic field and S_ℓ the power spectrum of the SV (Lowes, 1974), which are defined by

$$R_\ell = (\ell+1)\left(\frac{a}{r}\right)^{2\ell+4}\sum_{m=0}^{\ell}\left[\left(g_\ell^m\right)^2 + \left(h_\ell^m\right)^2\right] \tag{9}$$

$$S_\ell = (\ell+1)\left(\frac{a}{r}\right)^{2\ell+4}\sum_{m=0}^{\ell}\left[\left(\dot{g}_\ell^m\right)^2 + \left(\dot{h}_\ell^m\right)^2\right] \tag{10}$$

where r is the radius, ℓ and m the degree and order of spherical harmonics, g_ℓ^m and h_ℓ^m the Gauss coefficients of the magnetic field, and $\dot{g}_\ell^m$ and $\dot{h}_\ell^m$ the Gauss coefficients of the SV. An inverse linear relationship between τ_ℓ and ℓ was found for the non-dipole part of the spectrum in geomagnetic field models and numerical dynamo simulations (Christensen and Tilgner, 2004; Lhuillier et al., 2011; Bouligand et al., 2016; Amit et al., 2018; Tsang and Jones, 2024)

$$\tau_\ell = \frac{\tau_{SV}}{\ell} \tag{11}$$

where τ_{SV} is a constant. This relation is expected based on magnetic induction theory if the SV is dominated by advection (Christensen et al., 2012). Combining (8) and (11) and representing R_ℓ by $\mathscr{B}_\ell^2$ and S_ℓ by $\dot{\mathscr{B}}_\ell^2$, where $\mathscr{B}_\ell$ and $\dot{\mathscr{B}}_\ell$ are typical degree-dependent radial field and SV scales, gives

$$|\dot{\mathscr{B}}_\ell| \quad = \frac{\ell|\mathscr{B}_\ell|}{\tau_{SV}}. \tag{12}$$

$|\dot{\mathscr{B}}_\ell|$ is our proposed SV index which we term below T_i, and $|\mathscr{B}_\ell|$ is a proxy to the radial field B_r. In terms of the Gauss coefficients, Eq. (12) then becomes

$$T_i = \frac{\left|\sum_{\ell=1}^{\infty}\left(\frac{a}{r}\right)^{\ell+2}\ell(\ell+1)\sum_{m=0}^{\ell}\left[\left(g_\ell^m\cos m\phi + h_\ell^m\sin m\phi\right)\right]P_\ell^m\right|}{\tau_{SV}}, \tag{13}$$

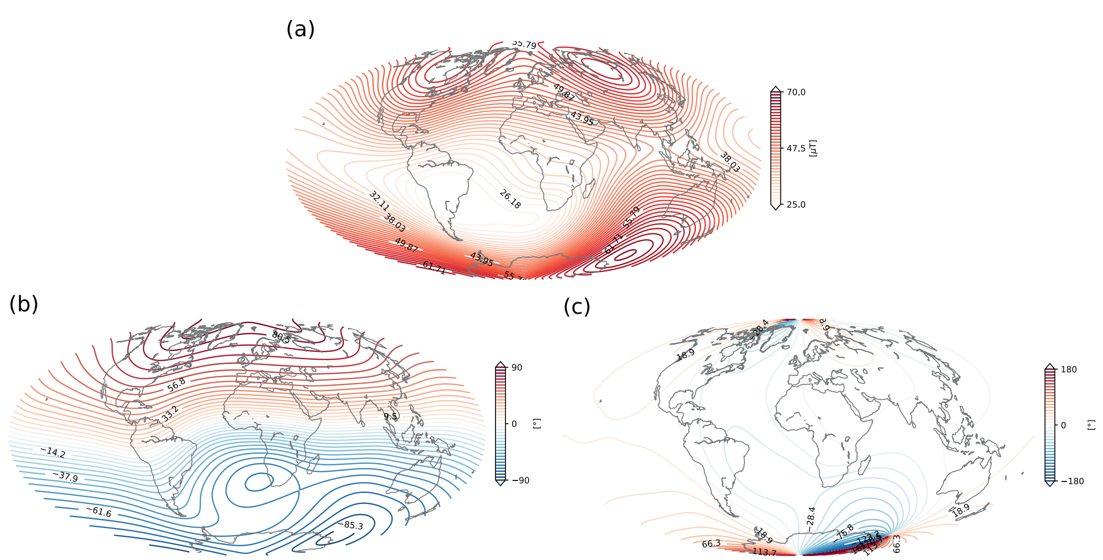

Fig. 2. Surface intensity (a), inclination (b) and declination (c) in the year 2010 based on the geomagnetic field model COV-OBS.x2 (Huder et al., 2020).

with P_ℓ^m the associated Legendre polynomials for degree ℓ and order m. Note the additional degree ℓ in (12) and (13) compared to simply B_r. Also note that we include the dipole in (13) despite the fact that (11) holds only for the non dipole. In practice, the additional factor ℓ in (13) renders the dipole secondary in T_i. We used $\tau_{SV} = 400$ yr which is the present day value (Amit et al., 2018). However, because we are interested mainly in large-scale SV patterns rather than magnitudes, this choice is not important. Moreover, in this study, we focus on hemispherical ratios, so τ_{SV} is canceled.

2.3. Hemispherical secular variation ratios

Two hemispherical SV ratios are calculated to test the reliability of the two indices and to monitor changes in the field hemispherical dichotomies in ancient times. We calculated the ratio of the northern hemisphere SV to the southern hemisphere SV (*NH*/*SH*) and the ratio of the Pacific hemisphere SV to the Atlantic hemisphere SV (*Pa*/*At*):

$$NH \Big/ SH = \frac{\int_{\phi=0}^{2\pi} \int_{\theta=0}^{\pi/2} \mathscr{X}(\phi\theta)\sin\theta \mathrm{d}\phi \mathrm{d}\theta}{\int_{\phi=0}^{2\pi} \int_{\theta=\pi/2}^{\pi} \mathscr{X}(\phi\theta)\sin\theta \mathrm{d}\phi \mathrm{d}\theta} \tag{14}$$

$$Pa \Big/ At = \frac{\int_{\phi=\pi/2}^{3\pi/2} \int_{\theta=0}^{\pi} \mathscr{X}(\phi\theta)\sin\theta \mathrm{d}\phi \mathrm{d}\theta}{\int_{\phi=0}^{\pi/2} \int_{\theta=0}^{\pi} \mathscr{X}(\phi\theta)\sin\theta \mathrm{d}\phi \mathrm{d}\theta + \int_{\phi=3\pi/2}^{2\pi} \int_{\theta=0}^{\pi} \mathscr{X}(\phi\theta)\sin\theta \mathrm{d}\phi \mathrm{d}\theta} \tag{15}$$

In (14) and (15) $\mathscr{X}$ is either the true absolute |SV|, P_i or T_i. In (15) We naively set the limits between the Pacific and Atlantic hemispheres to 90°W and 90°E. We examined the sensitivity of the results to this choice by also considering the limits 100°W and 80°E and 80°W and 100°E.

3. Results

3.1. Historical era

The maps of the true secular variation density |SV| and the indices P_i and T_i for the year 2010 based on the COV-OBS.x2 model (Huder et al., 2020) expanded until spherical harmonic degree $\ell_{max} = 14$ are shown in Fig. 3. The true |SV| is characterized by a small-scale pattern covering most of the Atlantic hemisphere (Fig. 3a), whereas P_i is characterized by much larger scales (Fig. 3b). In particular, P_i is concentrated in the region below the South Atlantic Ocean. In contrast, our new index T_i captures well the scale of the true |SV| as well as its spatial distribution. In particular T_i recovers well the strong |SV| structures at high latitudes of the northern hemisphere (see Fig. 1b for polar views) and at mid latitudes of the southern hemisphere (Fig. 3c).

The much better recovery of |SV| by T_i compared to P_i is further evident when examining averages of the three quantities vs. latitude and longitude (Fig. 4). Fig. 4a demonstrates that P_i is clearly concentrated in the southern hemisphere, whereas the true |SV| seems to show a more active northern hemisphere with a peak |SV| (8 μT.yr^{-1}) at 70°N. In the northern hemisphere, T_i predicts the true |SV| very well, including the high latitude peak, the polar low and the mild values elsewhere. However, in the southern hemisphere T_i predicts a strong |SV| peak around 70°S which is absent in the true |SV|. In the longitude averages (Fig. 4b), the true |SV| is stronger in the Atlantic hemisphere. The two indices also indicate a more active Atlantic hemisphere. However, P_i is very smooth whereas T_i varies with a similar azimuthal scale as the true |SV|.

Next, we calculated the values of the *NH*/*SH* (northern/southern hemisphere, (14)) and *Pa*/*At* (Pacific/Atlantic hemisphere, (15)) SV ratios in the year 2010 based on the COV-OBS.x2 model with $\ell_{max} = 14$ (Huder et al., 2020). We found that the *NH*/*SH* ratio based on T_i (1.09) is much closer to the true |SV| ratio (1.12) than the ratio based on P_i (0.39) (Fig. 4a). Moreover, $NH/SH > 1$ based on |SV| and T_i, i.e., stronger SV in the northern hemisphere, whereas the ratio is well below unity based on

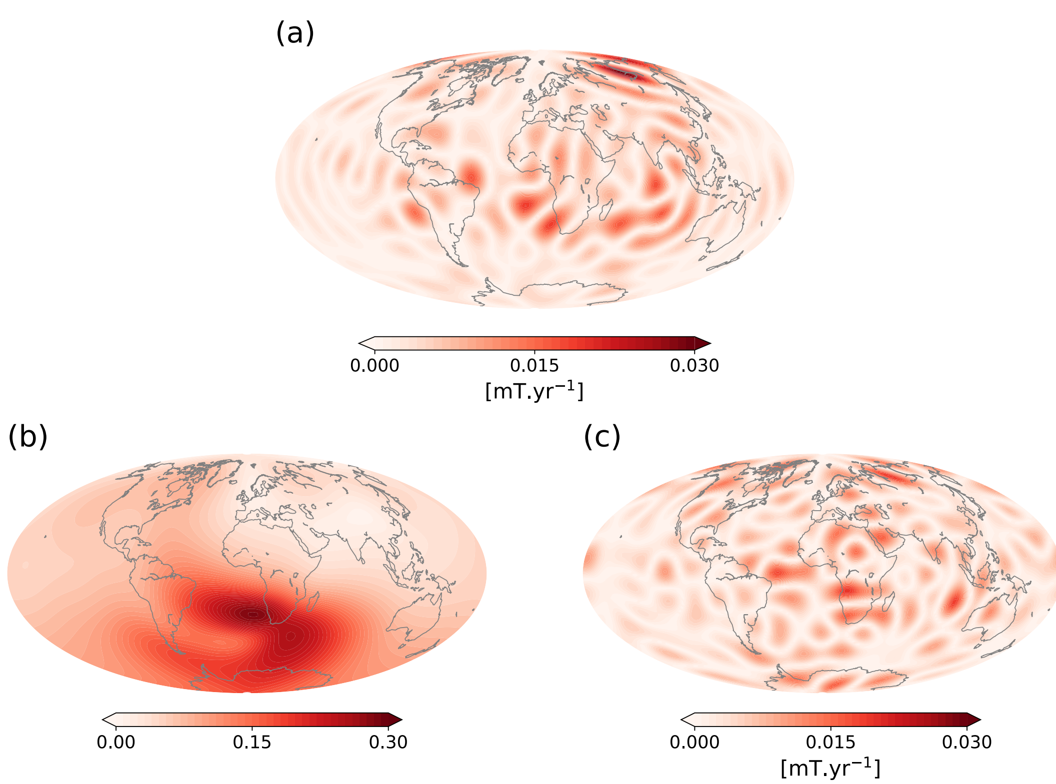

Fig. 3. Absolute geomagnetic SV at the CMB (a), P_i at Earth's surface (b) and T_i at the CMB (c) in the year 2010 based on the model COV-OBS.x2 until $\ell_{max} = 14$ (Huder et al., 2020).

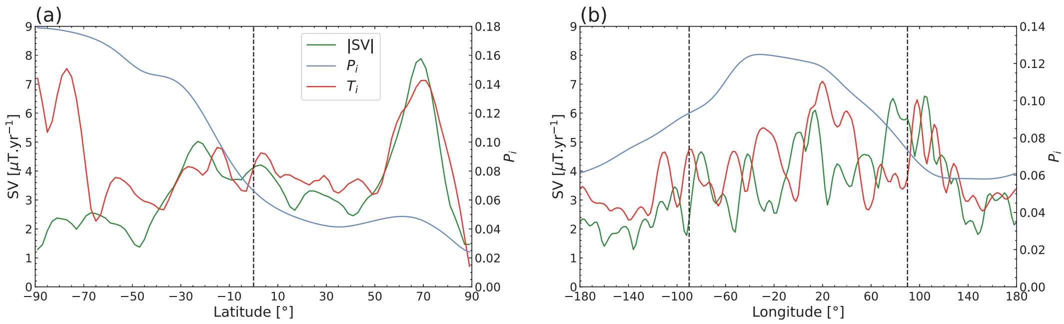

Fig. 4. Latitude (a) and longitude (b) averages of the true |SV| and the two indices in the year 2010. The green curves correspond to the averages calculated from Fig. 3a, the blue curves from Fig. 3b and the red curves from Fig. 3c. Dashed vertical lines correspond to the equator (a) and the limits between the Atlantic and Pacific hemispheres (b). The |SV| and T_i scales are on the left, the P_i scale is on the right. (For interpretation of the references to colour in this figure legend, the reader is referred to the web version of this article.)

P_i. The Pa/At ratios based on both indices (P_i and T_i) are close to the true |SV| ratio (0.71), with T_i (0.77) being slightly closer than P_i (0.62) (Fig. 4b).

In the next Section (3.2) we explore the prediction of our index for the past 100 kyr. The spatial resolution in paleomagnetic field models (e.g. GGF100k for the past 100,000 years) is significantly lower than in models of the historical field (e.g. COV-OBS.x2 for the period 1840–2020). This is manifested by the white non-dipole field power spectrum for the historical field as opposed to the sharp decrease in power beyond degree 5 for paleomagnetic field models (see Fig. 5 of Panovska et al., 2018b). It is therefore important to test the sensitivity of the results to the spatial resolution. Fig. 5 shows how the hemispherical ratios change as a function of the maximum spherical harmonic degree ℓ_{max} for two snapshots (1850 and 2010). Because the surface field is not strongly affected by higher degree contributions, P_i shows no dependence on ℓ_{max}. In contrast, for the true |SV| and T_i, the NH/SH and Pa/At ratios depend on ℓ_{max}. For the NH/SH ratio for the two snapshots and for all ℓ_{max} values T_i and the true |SV| which are evaluated on the CMB are comparable (Fig. 5a and b), whereas P_i is much smaller (i.e. too biased to the south). For the Pa/At ratio (Fig. 5c and d), |SV| and T_i present a similar dependence on ℓ_{max} (especially in 1850) while again P_i is too low (i.e. biased towards the Atlantic hemisphere). Most importantly for our purposes, no apparent deterioration in the recovery of the hemispherical ratios by T_i from $\ell_{max} = 14$ to 5 is observed. However, the agreement between T_i and |SV| for the Pa/At ratio is lost for $\ell_{max} = 3$.

We also tested the sensitivity of the resulting Pa/At ratio to the choice of limits between the Atlantic and Pacific hemispheres (dashed colored lines in Fig. 5c and d) by shifting these limits either 10° to the west or 10° to the east. These shifted limits of the Pacific and Atlantic hemispheres do not significantly affect the overall results, except for some particular cases (e.g. |SV| in 2010 for large ℓ_{max} or T_i in 1850 for $\ell_{max} = $ 6-8).

Next, we calculated the two hemispherical SV ratios for the entire period covered by the COV-OBS.x2 model (Huder et al., 2020) for two

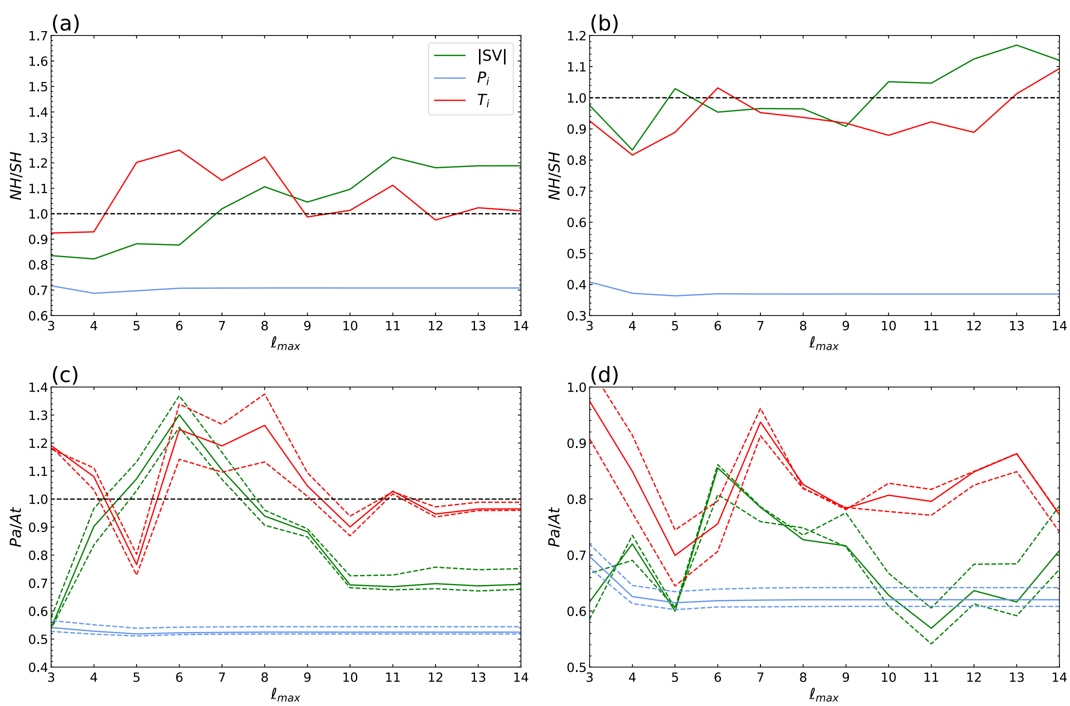

Fig. 5. Hemispherical ratios as a function of the maximum degree of spherical harmonics for the COV-OBS.x2 model (Huder et al., 2020). (a) and (c) correspond to the year 1850 and (b) and (d) to the year 2010. The green curves correspond to the true |SV| model, the blue curves to P_i and the red curves to T_i. Dashed horizontal black lines denote no hemispherical dichotomy. Dashed colored lines in (c) and (d) denote Pa/At ratios based on alternative limits between the Atlantic and Pacific hemispheres at [80°W,100°E] and [100°W,80°E]. (For interpretation of the references to colour in this figure legend, the reader is referred to the web version of this article.)

different truncations: $\ell_{max} = 5$ (Fig. 6a and c) corresponding to the typical archeomagnetic spatial resolution and $\ell_{max} = 14$ (Fig. 6b and d) corresponding to the historical field's spatial resolution. The ratios based on |SV| are characterized by high frequency oscillations whereas based on P_i and T_i the ratios are very smooth. For the NH/SH ratio for the two values of ℓ_{max} (5 and 14) T_i recovers better the |SV| average values (Table 1) and the long-term trends (Fig. 6a and b). For the Pa/At ratio, for both values of ℓ_{max}, T_i shows a similar trend as the true |SV| whereas P_i has an increasing trend opposite to the true |SV| (Fig. 6c and d). However, for $\ell_{max} = 14$ the average Pa/At value of P_i is closer to the true |SV| value (Table 1).

To further illustrate the performance of the SV indices we examine two snapshots of the COV-OBS.x2 model, corresponding to two specific and distinctive SV configurations. The first snapshot corresponds to the year 1920 (Fig. 7 left column), when the NH/SH and Pa/At ratios for the true |SV| with $\ell_{max} = 14$ are the lowest (Fig. 6b and d). At this snapshot, the true |SV| is strongest below the South Atlantic (Fig. 7b). These strong SV structures are related to the expansion, intensification and mobility of reversed geomagnetic flux patches (Fig. 7a). Here P_i predicts well the |SV| in the South Atlantic (Fig. 7c). In contrast, T_i predicts strong |SV| associated with the intense high-latitude geomagnetic flux patches (Fig. 7d) which are absent in the true |SV| (Fig. 7b).

The second snapshot corresponds to the year 1892 (Fig. 7 right column and Fig. 8) when the true |SV| Pa/At ratio is largest and very close to 1 (Fig. 6d), i.e., the SV intensity in the Atlantic hemisphere is comparable to that in the Pacific. The true |SV| indeed includes some strong structures in the Pacific hemisphere, e.g. below south west Patagonia and the Bering sea (Fig. 7f). P_i fails to predict these Pacific SV features (Fig. 7h). Instead P_i still shows a strong southern Atlantic dominance (Fig. 8b). In contrast, T_i recovers well these pacific SV features (Figs. 7g and 8b). For this snapshot, the Pa/At ratio based on T_i is 0.91, close to the true |SV| ratio (0.99, see Fig. 6d).

Table 1
Hemispherical ratios in the true |SV| and based on the two indices P_i and T_i for different geomagnetic field models. ℓ_{max} is the maximum degree of spherical harmonic of each model. The values of |SV|, P_i and T_i correspond to the mean over the entire period covered by each model with the standard deviation representing time dependence.

Model	COV-OBS.x2	COV-OBS.x2	GGF100k	pfm9k.2
Period	1840 - 2020	1840 - 2020	−98150 - 1850	−7000 - 1850
Time step [yr]	2	2	200	50
Ref.	Huder et al. (2020)	Huder et al. (2020)	Panovska et al. (2018b)	Nilsson et al. (2022)
ℓ_{max}	14	5	10	5
North/South hemisphere ratio				
|SV|	1.03 ± 0.11	0.85 ± 0.16		
P_i	0.52 ± 0.10	0.52 ± 0.10	0.88 ± 0.31	1.06 ± 0.34
T_i	1.11 ± 0.09	1.00 ± 0.09	1.41 ± 0.48	1.38 ± 0.27
Pacific/Atlantic hemisphere ratio [90°W - 90°E]				
|SV|	0.69 ± 0.14	0.70 ± 0.14		
P_i	0.59 ± 0.04	0.59 ± 0.04	0.88 ± 0.29	0.95 ± 0.40
T_i	0.88 ± 0.07	0.75 ± 0.03	0.75 ± 0.21	1.01 ± 0.23
Pacific/Atlantic hemisphere ratio [100°W - 80°E]				
|SV|	0.73 ± 0.13	0.72 ± 0.14		
P_i	0.58 ± 0.04	0.58 ± 0.04	0.86 ± 0.28	0.94 ± 0.39
T_i	0.87 ± 0.06	0.75 ± 0.02	0.74 ± 0.20	0.99 ± 0.21
Pacific/Atlantic hemisphere ratio [80°W - 100°E]				
|SV|	0.68 ± 0.14	0.70 ± 0.12		
P_i	0.62 ± 0.04	0.61 ± 0.04	0.92 ± 0.30	0.95 ± 0.40
T_i	0.88 ± 0.10	0.73 ± 0.05	0.77 ± 0.20	1.03 ± 0.24

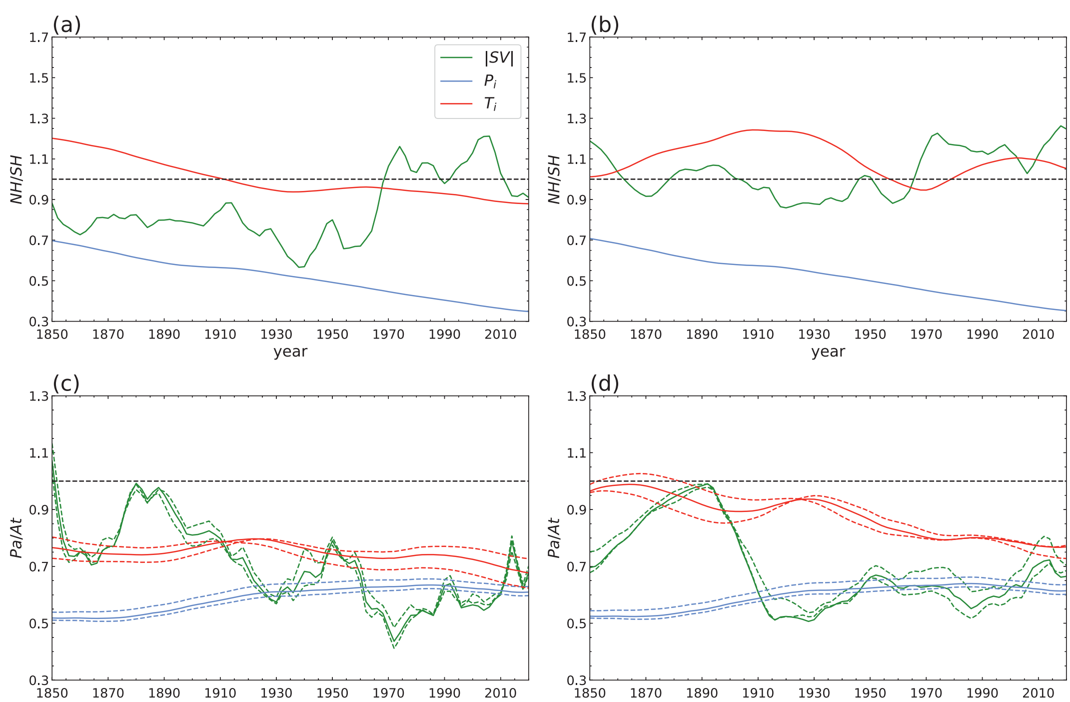

Fig. 6. Hemispherical ratios as a function of time for the COV-OBS.x2 model (Huder et al., 2020). (a) and (c) correspond to $\ell_{max} = 5$ and (b) and (d) to 14. The green curves correspond to the true |SV| model, the blue curves to P_i and the red curves to T_i. Dashed horizontal black lines denote no hemispherical dichotomy. Dashed colored lines in (c) and (d) denote possible alternative limits between the Atlantic and Pacific hemispheres at [80°W,100°E] and [100°W,80°E]. (For interpretation of the references to colour in this figure legend, the reader is referred to the web version of this article.)

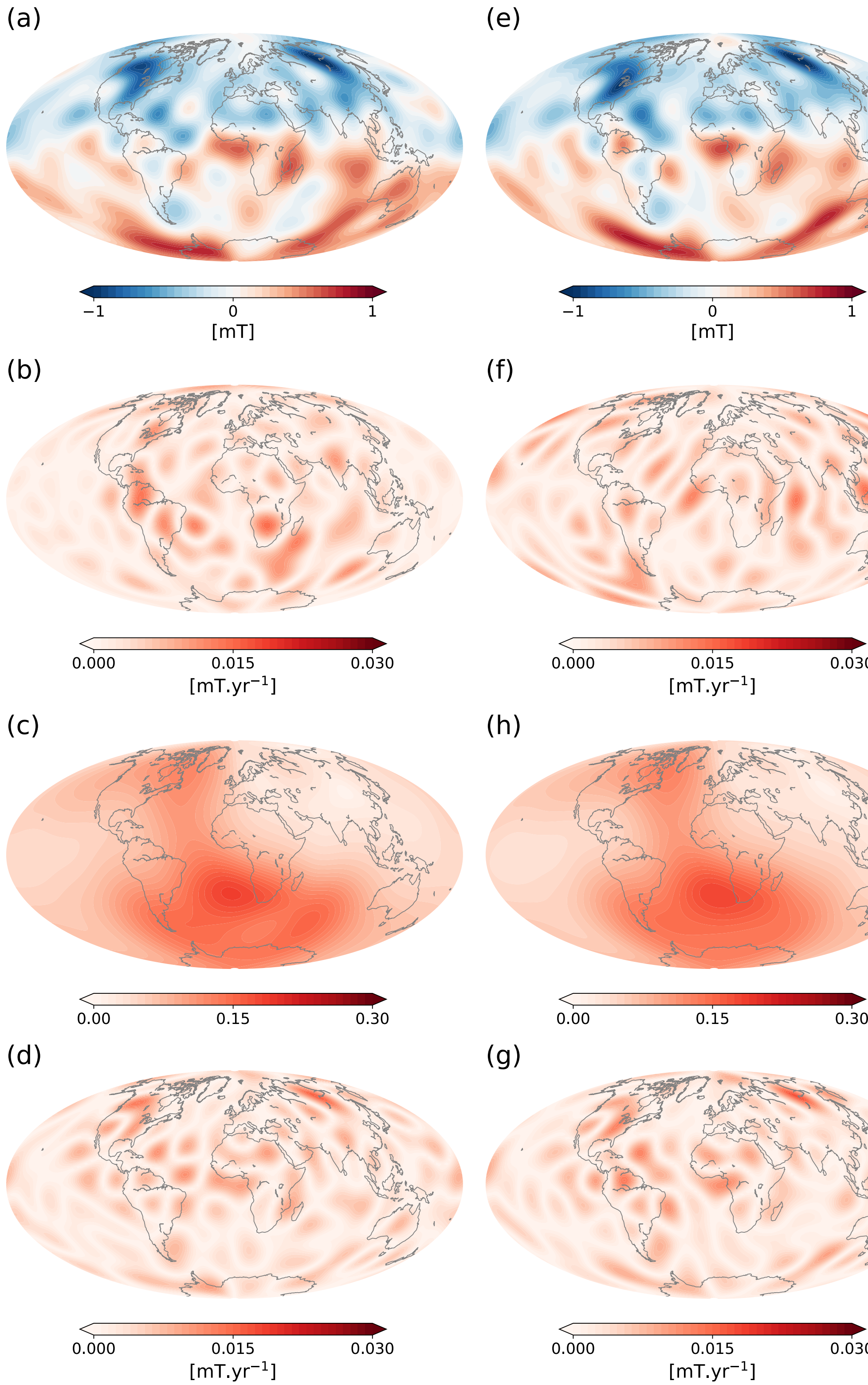

Fig. 7. The radial component of the geomagnetic field (a) and (e), the true |SV| (b) and (f), P_i (c) and (h) and T_i (d) and (g) in the year 1920 (left) and 1892 (right) based on COV-OBS.x2 (Huder et al., 2020) with $\ell_{max} = 14$. The year 1920 corresponds to the time when the NH/SH and Pa/At ratios based on |SV| are at their lowest for the period 1840–2020: $NH/SH = 0.86$ and $Pa/At = 0.52$. The year 1892 corresponds to the time when the Pa/At ratio based on |SV| is close to 1.

3.2. Holocene and late Pleistocene epochs

Next, the two indices, P_i (4) and T_i (13), were applied for two geomagnetic field models of the past: GGF100k of Panovska et al. (2018b) which covers the last 100,000 years and pfm9k.2 of Nilsson et al. (2022) which covers the last 9000 years. The ratios NH/SH (14) and Pa/At (15) based on the P_i and T_i indices and their associated standard deviations for both models are given in Table 1.

Fig. 9a and b show the results for the NH/SH and Pa/At hemispherical SV ratios over the entire period covered by the GGF100k

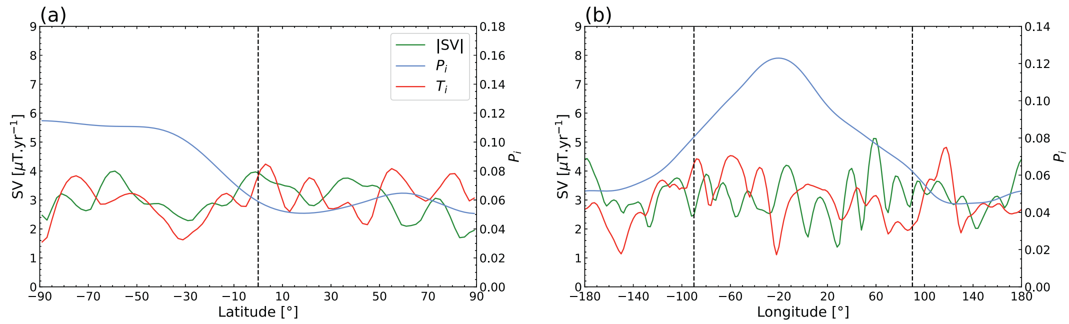

Fig. 8. As in Fig. 4 for the year 1892.

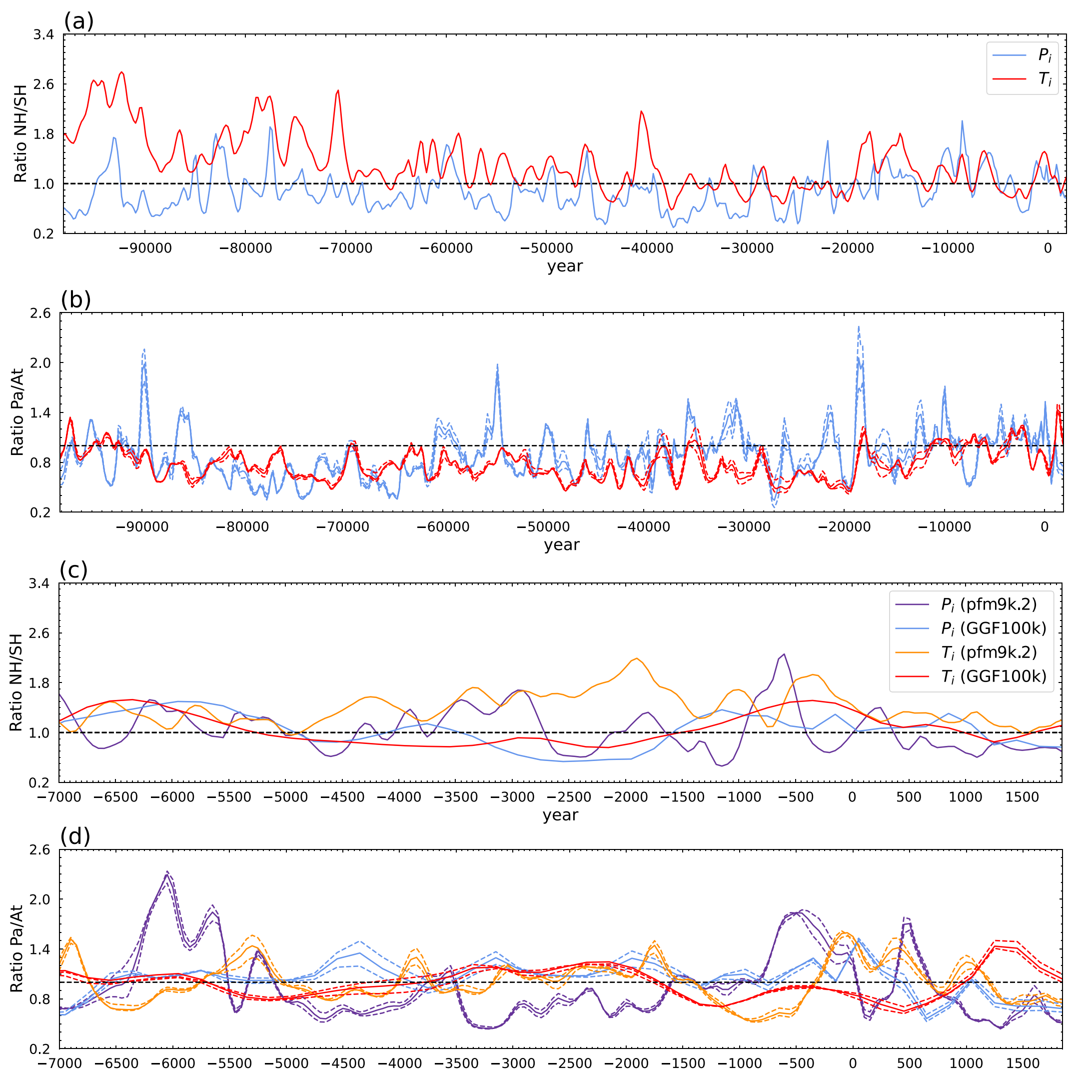

Fig. 9. Hemispherical ratios based on P_i and T_i for the past 100 kyr with the paleomagnetic field model GGF100k (Panovska et al., 2018b) and for the past 9 kyr with the archeomagnetic field model pmf9k.2 (Nilsson et al., 2022). Dashed horizontal black lines denote no hemispherical dichotomy. Dashed colored lines in (b) and (d) denote alternative limits between the Atlantic and Pacific hemispheres at [80°W,100°E] and [100°W,80°E].

model (Panovska et al., 2018b) based on P_i and T_i. According to the T_i index, in the past, the |SV| was strongly localized in the northern hemisphere, reaching a peak NH/SH ratio of 3.05 in the year −92,150 (Fig. 9a). A southern hemisphere-dominant pattern occurred rarely over the last 100,000 years. On average based on T_i the |SV| was ∼ 40% stronger in the northern hemisphere than in the southern (Table 1). In contrast, P_i indicates a slight preference for the southern hemisphere (Fig. 9a and Table 1). Note that caution should be taken in particular when interpreting the large NH/SH values based on T_i for the early period due to the decrease in paleomagnetic data availability prior to the year −60,000 (see Fig. 1b of Panovska et al., 2018b).

In addition, T_i presents a dominance of SV activity in the Atlantic hemisphere (Fig. 9b). The average Pa/At ratio over the past 100,000 years based on T_i is very similar to that of T_i based on the historical field with $\ell_{max} = 5$ (Table 1). Moreover, based on T_i a more pronounced Pacific hemisphere |SV| occurred seldom (Fig. 9b). P_i shows the same trend as T_i, i.e., on average, a dominance of SV activity in the Atlantic hemisphere, but events of Pacific hemisphere dominance are more often with P_i than with T_i and the average Atlantic dominance based on P_i is less pronounced (Table 1).

To compare with an alternative model, a zoom into the past 9 kyr (Fig. 9c and d) was carried out using the pfm9k.2 model of Nilsson et al. (2022). We find that for NH/SH, the ratios of T_i are always greater than or equal to 1 (Fig. 9c) with a large average value of 1.38 (see Table 1) indicating that over this period the northern hemisphere has always dominated the |SV|. Based on P_i the NH/SH values over the last 9 kyr have oscillated around 1 (average of 1.06, see Table 1) indicating no persistent dichotomy between the northern and southern hemispheres |SV| during this period. Both P_i and T_i indicate that the dichotomy between the Pacific and Atlantic hemispheres in the last 9 kyr was not persistent (average of 0.95 for P_i and 1.01 for T_i, Fig. 9d and Table 1). However, large temporal variations in Pa/At are found. Changing the position of the limits between the Pacific/Atlantic hemispheres for calculating the Pa/At ratio in the paleomagnetic and archeomagnetic field models (dashed colored lines in Fig. 9b and d) has very little influence on the values of P_i and T_i (Fig. 9b and d and Table 1).

To illustrate the way the indices capture scenarios of extreme hemispherical dichotomies, two snapshots of B_r, P_i and T_i are presented from the GGF100k model. The first snapshot (Fig. 10 left column) corresponds to the time when the difference of the NH/SH ratio between T_i and P_i is the highest, which occurred at −91,750. At this year, the value of NH/SH based on T_i indicates a northern hemisphere dominance ($NH/SH > 1$) whereas based on P_i a southern hemisphere dominance ($NH/SH < 1$) is expected. For this snapshot T_i (Fig. 10c) predicts strong |SV| at locations where the radial field is intense and small-scale (Fig. 10a). In contrast, P_i (Fig. 10b) predicts significant |SV| where B_r is particularly weak and characterized by large-scale structures (southern hemisphere, Fig. 10a).

The second snapshot (Fig. 10 right column) corresponds to the year 1850 when the Pa/At ratio based on T_i is highest ($Pa/At = 1.53$). For this snapshot, T_i shows strong localization of |SV| in the form of three patches around longitude 110°E (Fig. 10f) where intense small-scale B_r patches prevail (Fig. 10d). Based on P_i, this ratio is much smaller ($Pa/At = 0.71$), with a strong |SV| below the Atlantic Ocean (Fig. 10e) where the field is either reversed (e.g. under Patagonia) or large scale (e.g. under North America) (Fig. 10d).

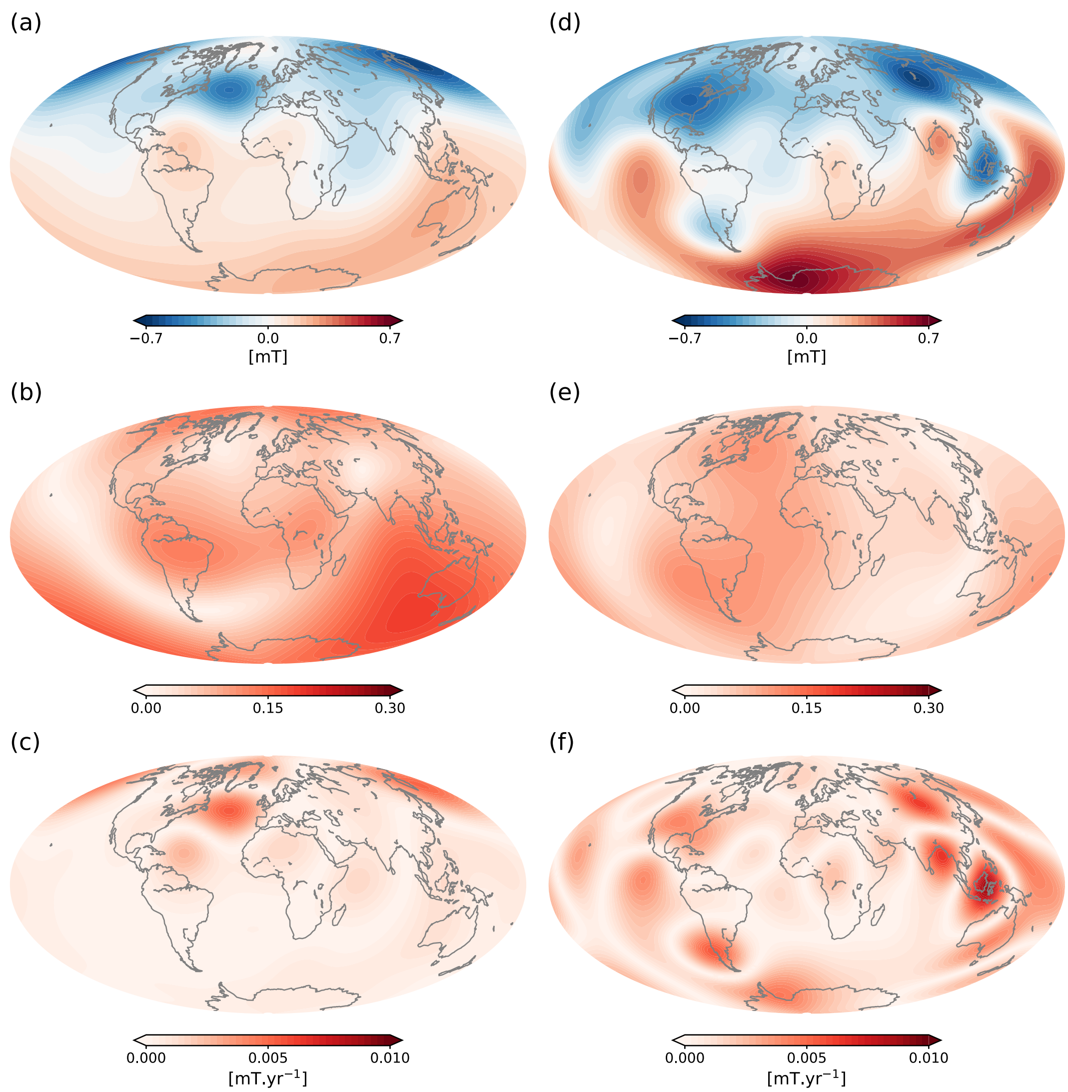

Fig. 10. The radial component of the geomagnetic field (a) and (d), P_i (b) and (e) and T_i (c) and (f) for the years −91,750 (left) and 1850 (right) based on GGF100k (Panovska et al., 2018b). These years correspond to times when the North/South hemispherical ratio is strongest for T_i (left) and when the Pacific/Atlantic hemispherical ratio is strongest for T_i (right), for the entire period of the GGF100k model of Panovska et al. (2018b).

4. Discussion

We propose a new index for the paleomagnetic SV. In the context of reproducing the pattern of |SV| on the CMB, based on tests with the historical field model in which the SV is known, this new index, which we termed T_i, performs much better than the previously proposed index, P_i. Our new index is based on a well-established scaling law for the degree dependence of SV timescales (Lhuillier et al., 2011). The main differences between P_i and our index T_i are (1) P_i is based on the field at the surface whereas T_i is based on the field at the CMB and (2) P_i measures the deviations from axial dipole (4) whereas T_i accounts for the overall degree dependence of the SV (13). Consequently, P_i is large where the field is weak or reversed, whereas T_i is large where the field is strong and concentrated, i.e., where ∇B_r is large, hence there is a potential for intense SV (Fig. 10). These fundamental differences between the two indices suggest that T_i is more adequate for reproducing the spatial pattern of |SV| than P_i. In particular T_i reproduces small-scale structures (Fig. 3c), which are characteristic of the |SV| (Fig. 3a), whereas P_i is very large scale (Fig. 3b).

Note that T_i is not expected to precisely reproduce the structures of |SV| because a moving field patch induces a pair of opposite-sign upwind and downwind SV patches (Amit, 2014) hence a slight shift is expected between the T_i and true |SV| patterns. However, in the context of large-scale features such as hemispherical SV patterns, T_i is adequate. Indeed, at present T_i fits the true |SV| very well (Figs. 3 and 4a), especially in the northern hemisphere and at low latitudes of the southern hemisphere. In contrast, P_i is strongly biased towards the southern hemisphere (Figs. 3 and 4a). This superior representation of |SV| by T_i is also evident in the NH/SH and Pa/At ratios (Table 1). For the historical era, the average NH/SH ratio based on T_i is very close to that of the true |SV|, in contrast to that of P_i. For Pa/At and $\ell_{max} = 14$, P_i performs better than T_i, but with $\ell_{max} = 5$, which roughly corresponds to the spatial resolution of archeomagnetic field models covering the past three millennia (e.g. Licht et al., 2013; Sanchez et al., 2016), T_i performs much better than P_i (Table 1).

For $\ell_{max} = 3$ the agreement between Ti and |SV| concerning the Pa/At ratio is lost. However, the validity of our analysis relies on the robustness of the paleomagnetic field model until $\ell_{max} = 5$. The amount of paleomagnetic data increases gradually in time towards present (see Fig. 1b of Panovska et al., 2018b). In particular, there is significantly more data during the Holocene than before this epoch. However, most archeomagnetic field models covering the Holocene either use a limited amount of sediment data which comprises by far the largest portion of the database (Nilsson et al., 2014, 2022; Constable et al., 2016) or do not use any sediment data at all (Pavón-Carrasco et al., 2014; Arneitz et al., 2019; Campuzano et al., 2019; Schanner et al., 2022). In contrast, Panovska et al. (2018a) added a new compilation of sediment dataset. This new dataset served to construct the 100 kyr model of Panovska et al. (2018b). The GGF100k model is heavily constrained by more than 100 continuous sediment records covering extended periods of time. Consequently, the GGF100k model resolves comparable spatial power (practically up to spherical harmonic degree and order 5) though less temporal complexity compared to Holocene geomagnetic field models (Panovska et al., 2018b). Indeed, since published this model has been broadly used to infer the properties of the geomagnetic field over the past 100 kyr (e.g. Davies and Constable, 2020; Meduri et al., 2021; Korte et al., 2022; Mound and Davies, 2023; Constable and Davies, 2024; Mason et al., 2024).

In the year 2010 a discrepancy between the true |SV| and T_i is observed at high latitudes of the southern hemisphere (Fig. 4a). Here, T_i predicts an intense peak in |SV| but the true |SV| is weak. The strong |SV| peak at northern high latitudes in both the true |SV| and T_i is explained by the presence of a powerful zonal jet there (Livermore et al., 2017). According to rapid rotation theory, the core dynamics are in a quasi-geostrophic force balance, i.e., the flow is expected to be symmetric about the equator (e.g. Busse, 1970; Jault, 2008). The powerful jet at high northern latitudes should therefore also be present at the corresponding high southern latitudes. The absence of a peak in the true |SV| at southern high latitudes (Fig. 1b) may arise because the flow is parallel to contours of the radial magnetic field (Finlay and Amit, 2011), resulting in no magnetic induction by advection there (Livermore et al., 2017). The false peak in T_i at high southern latitudes may therefore be an outcome of a field-flow alignment effect that is not accounted for in T_i. At other times, this discrepancy does not prevail and T_i reproduces well |SV| at all latitudes (Fig. 8a).

The spatial resolution test of the two indices for the two hemispherical ratios (Fig. 5) demonstrates that T_i recovers better the true |SV| for ℓ_{max} in the range 5–14, while P_i is very often below the true |SV| values (i.e. biased to the southern and Atlantic hemispheres). This test also indicates that P_i does not depend on ℓ_{max} as this index is determined at the surface, in contrast to T_i which is defined on the CMB just as the true |SV|. Importantly T_i does not exhibit any deterioration of |SV| recovery from $\ell_{max} = 14$ to 5. Fig. 6 shows, however, that in terms of time dependency, both indices fail to capture the high frequency oscillations of the true |SV|. The reason is possibly that core flow is not accounted for explicitly in T_i.

Calculation of the Pa/At ratio based on T_i over the last 100 kyr (GGF100k; Panovska et al., 2018b) demonstrates that the Pacific-Atlantic |SV| dichotomy observed today is a phenomenon that persisted in the past (Fig. 9). The average Pa/At ratio based on T_i for the last 100 kyr is 0.75, in striking agreement with the observed true |SV| and T_i values for the historical era (Table 1), which may be fortuitous. This finding contradicts the results of Mound and Davies (2023) who, using P_i, argued that this dichotomy is merely a recent phenomenon and that in the past the Pa/At ratio was close to 1. They concluded that the scenario of geodynamo control by heterogeneous inner core freezing (Aubert et al., 2013) should therefore be ruled out. Our finding, based on T_i, indicates that this hemispherical Pacific/Atlantic SV dichotomy is a long-term persistent feature of the geodynamo, in agreement with heterogeneous inner core freezing as a plausible scenario for explaining the observed geomagnetic SV, as well as in agreement with an evaluation of the paleomagnetic SV over the past 10 Myrs (Engbers et al., 2020; de Oliveira et al., 2024).

In contrast, the analysis of the pfm9k.2 model (Nilsson et al., 2022) does not indicate the presence of a Pacific/Atlantic SV dichotomy (Fig. 9d). There are two possible reasons for this discrepancy. One possibility is that the pfm9k.2 model is more robust because prior to 10 kyr the limited constraints on the absolute strength of the Earth's magnetic field mostly rely on the relative paleointensity estimates from sediments rather than absolute paleointensity experiments from volcanic or baked clays. Alternatively, the paleomagnetic field model GGF100k covers a significantly longer period, hence its analysis is more statistically meaningful in terms of depicting the persistent features of the geomagnetic field.

The P_i index is useful when only measurement points are available (Panovska and Constable, 2017) since it does not require a global archeomagnetic or paleomagnetic model as our new SV index T_i. Moreover, P_i highs correlate very well with reversals and excursions (Panovska and Constable, 2017; Korte et al., 2019; Mahgoub et al., 2024). However, for recovery of the spatial pattern of |SV| at the CMB we find that T_i is more adequate. Analysis of future paleomagnetic field models that will be constructed from an increasing database may confirm or dispute our finding concerning the long-term nature of the Pacific/Atlantic dichotomy in Earth's magnetic SV.

CRediT authorship contribution statement

Mathis Colas: Writing – original draft, Visualization, Software, Methodology, Investigation, Formal analysis, Data curation. **Filipe Terra-Nova:** Writing – review & editing, Supervision, Methodology, Investigation, Formal analysis, Data curation. **Hagay Amit:** Writing – review & editing, Validation, Supervision, Project administration, Methodology, Funding acquisition, Conceptualization.

Author agreement

We wish to confirm that there are no known conflicts of interest associated with this publication and there has been no significant financial support for this work that could have influenced its outcome. We confirm that the manuscript has been read and approved by all named authors and that there are no other persons who satisfied the criteria for authorship but are not listed. We further confirm that the order of authors listed in the manuscript has been approved by all of us. We confirm that we have given due consideration to the protection of intellectual property associated with this work and that there are no impediments to publication, including the timing of publication, with respect to intellectual property. In so doing we confirm that we have followed the regulations of our institutions concerning intellectual property.

We understand that the Corresponding Author is the sole contact for the Editorial process (including Editorial Manager and direct communications with the office). He is responsible for communicating with the other authors about progress, submissions of revisions and final approval of proofs. We confirm that we have provided a current, correct email address which is accessible by the Corresponding Author.

Declaration of competing interest

The authors declare the following financial interests/personal relationships which may be considered as potential competing interests:

Hagay Amit reports financial support was provided by French National Research Agency. Filipe Terra-Nova reports financial support was provided by French Space Agency. If there are other authors, they declare that they have no known competing financial interests or personal relationships that could have appeared to influence the work reported in this paper.

Acknowledgement

We thank Patrick Arneitz and an anonymous reviewer for their useful comments. We acknowledge the financial support from the French Agence Nationale de Recherche, project DYRE-COMB (grant ANR-22-CE49-0016–01). F.T.-N. was supported by the Centre National d'Études Spatiales (CNES) under the project MIMES.

Data availability

Data will be made available on request.

References

Amit, H., 2014. Can downwelling at the top of the Earth's core be detected in the geomagnetic secular variation? Phys. Earth Planet. Inter. 229, 110–121.

Amit, H., Coutelier, M., Christensen, U.R., 2018. On equatorially symmetric and antisymmetric geomagnetic secular variation timescales. Phys. Earth Planet. Inter. 276, 190–201.

Arneitz, P., Egli, R., Leonhardt, R., Fabian, K., 2019. A Bayesian iterative geomagnetic model with universal data input: self-consistent spherical harmonic evolution for the geomagnetic field over the last 4000 years. Phys. Earth Planet. Inter. 290, 57–75.

Aubert, J., Finlay, C.C., Fournier, A., 2013. Bottom-up control of geomagnetic secular variation by the Earth's inner core. Nature 502, 219–223.

Backus, G., Parker, R.L., Constable, C., 1996. Foundations of Geomagnetism. Cambridge University Press.

Biggin, A.J., van Hinsbergen, D.J., Langereis, C.G., Straathof, G.B., Deenen, M.H., 2008. Geomagnetic secular variation in the cretaceous Normal Superchron and in the Jurassic. Phys. Earth Planet. Inter. 169, 3–19.

Bloxham, J., Gubbins, D., 1985. The secular variation of Earth's magnetic field. Nature 317, 777–781.

Bloxham, J., Jackson, A., 1991. Fluid flow near the surface of Earth's outer core. Rev. Geophys. 29, 97–120.

Bouligand, C., Gillet, N., Jault, D., Schaeffer, N., Fournier, A., Aubert, J., 2016. Frequency spectrum of the geomagnetic field harmonic coefficients from dynamo simulations. Geophys. Suppl. Mon. Not. R. Astron. Soc. 207, 1142–1157.

Busse, F.H., 1970. Thermal instabilities in rapidly rotating systems. J. Fluid Mech. 44, 441–460.

Butler, R.F., 1992. Paleomagnetism: magnetic domains to geologic terranes, 319. Blackwell Scientific Publications Boston.

Campuzano, S.A., Gómez-Paccard, M., Pavón-Carrasco, F.J., Osete, M.L., 2019. Emergence and evolution of the South Atlantic Anomaly revealed by the new paleomagnetic reconstruction SHAWQ2k. Earth Planet. Sci. Lett. 512, 17–26.

Christensen, U.R., Olson, P., 2003. Secular variation in numerical geodynamo models with lateral variations of boundary heat flow. Phys. Earth Planet. Inter. 138, 39–54.

Christensen, U.R., Tilgner, A., 2004. Power requirement of the geodynamo from ohmic losses in numerical and laboratory dynamos. Nature 429, 169–171.

Christensen, U.R., Wardinski, I., Lesur, V., 2012. Timescales of geomagnetic secular acceleration in satellite field models and geodynamo models. Geophys. J. Int. 190, 243–254.

Constable, C.G., Davies, C.J., 2024. Rapid changes in strength and direction of Earth's magnetic field over the past 100,000 years. Geochem. Geophys. Geosyst. 25 e2023GC011236.

Constable, C., Korte, M., Panovska, S., 2016. Persistent high paleosecular variation activity in southern hemisphere for at least 10 000 years. Earth Planet. Sci. Lett. 453, 78–86.

Cromwell, G., Johnson, C., Tauxe, L., Constable, C., Jarboe, N., 2018. PSV10: a global data set for 0–10 Ma time-averaged field and paleosecular variation studies. Geochem. Geophys. Geosyst. 19, 1533–1558.

Davies, C.J., Constable, C.G., 2020. Rapid geomagnetic changes inferred from Earth observations and numerical simulations. Nat. Commun. 11, 3371.

de Oliveira, W.P., Hartmann, G.A., Terra-Nova, F., Pasqualon, N.G., Savian, J.F., Lima, E. F., da Luz, F.R., Trindade, R.I.F., 2024. Long-term persistency of a strong non-dipole field in the South Atlantic. Nat. Commun. 15, 9447.

Dumberry, M., More, C., 2020. Weak magnetic field changes over the Pacific due to high conductance in lowermost mantle. Nat. Geosci. 13, 516–520.

Engbers, Y.A., Biggin, A.J., Bono, R.K., 2020. Elevated paleomagnetic dispersion at Saint Helena suggests long-lived anomalous behavior in the South Atlantic. Proc. Natl. Acad. Sci. 117, 18258–18263.

Finlay, C.C., Amit, H., 2011. On flow magnitude and field-flow alignment at Earth's core surface. Geophys. J. Int. 186, 175–192.

Finlay, C.C., Kloss, C., Olsen, N., Hammer, M.D., Tøffner-Clausen, L., Grayver, A., Kuvshinov, A., 2020. The CHAOS-7 geomagnetic field model and observed changes in the South Atlantic Anomaly. Earth Planets Space 72, 156.

Finlay, C.C., Gillet, N., Aubert, J., Livermore, P.W., Jault, D., 2023. Gyres, jets and waves in the Earth's core. Nat. Rev. Earth Environ. 4, 377–392.

Gauss, C.F., 1833. Intensitas vis magneticae terrestris ad mensuram absolutam revocata. Göttingen Comment 3–44.

Holme, R., 2015. Large-scale flow in the core. In: Olson, P. (Ed.), Treatise on Geophysics (Second Edition). Elsevier Science.

Holme, R., Olsen, N., Bairstow, F., 2011. Mapping geomagnetic secular variation at the core–mantle boundary. Geophys. J. Int. 186, 521–528.

Huder, L., Gillet, N., Finlay, C.C., Hammer, M.D., Tchoungui, H., 2020. COV-OBS. x2: 180 years of geomagnetic field evolution from ground-based and satellite observations. Earth Planets Space 72, 1–18.

Hulot, G., Le Mouël, J., 1994. A statistical approach to the Earth's main magnetic field. Phys. Earth Planet. Inter. 82, 167–183.

Hulot, G., Eymin, C., Langlais, B., Mandea, M., Olsen, N., 2002. Small-scale structure of the geodynamo inferred from Oersted and Magsat satellite data. Nature 416, 620–623.

Jault, D., 2008. Axial invariance of rapidly varying diffusionless motions in the Earth's core interior. Phys. Earth Planet. Inter. 166, 67–76.

Korte, M., Donadini, F., Constable, C., 2009. Geomagnetic field for 0–3 ka: 2. A new series of time-varying global models. Geochem. Geophys. Geosyst. 10.

Korte, M., Brown, M.C., Panovska, S., Wardinski, I., 2019. Robust characteristics of the Laschamp and Mono Lake geomagnetic excursions: results from global field models. Front. Earth Sci. 7, 86.

Korte, M., Constable, C.G., Davies, C.J., Panovska, S., 2022. Indicators of mantle control on the geodynamo from observations and simulations. Front. Earth Sci. 10, 957815.

Lhuillier, F., Fournier, A., Hulot, G., Aubert, J., 2011. The geomagnetic secular-variation timescale in observations and numerical dynamo models. Geophys. Res. Lett. 38.

Licht, A., Hulot, G., Gallet, Y., Thébault, E., 2013. Ensembles of low degree archeomagnetic field models for the past three millennia. Phys. Earth Planet. Inter. 224, 38–67.

Livermore, P.W., Hollerbach, R., Finlay, C.C., 2017. An accelerating high-latitude jet in Earth's core. Nat. Geosci. 10, 62–68.

Lowes, F., 1974. Spatial power spectrum of the main geomagnetic field, and extrapolation to the core. Geophys. J. Int. 36, 717–730.

Mahgoub, A.N., Korte, M., Panovska, S., Schanner, M., 2024. Robustness of characteristics of the Matuyama-Brunhes geomagnetic field reversal found in global models. Front. Earth Sci. 12, 1443095.

Mason, S.J., Davies, C.J., Clarke, A.T., Constable, C.G., 2024. Insights into the last 100 ky of geomagnetic field variability using numerical dynamo simulations. Earth Planet. Sci. Lett. 646, 119011.

Meduri, D., Biggin, A., Davies, C., Bono, R., Sprain, C., Wicht, J., 2021. Numerical dynamo simulations reproduce paleomagnetic field behavior. Geophys. Res. Lett. 48, e2020GL090544.

Mound, J.E., Davies, C.J., 2023. Longitudinal structure of Earth's magnetic field controlled by lower mantle heat flow. Nat. Geosci. 16, 380–385.

Nilsson, A., Holme, R., Korte, M., Suttie, N., Hill, M., 2014. Reconstructing Holocene geomagnetic field variation: new methods, models and implications. Geophys. J. Int. 198, 229–248.

Nilsson, A., Suttie, N., Stoner, J.S., Muscheler, R., 2022. Recurrent ancient geomagnetic field anomalies shed light on future evolution of the South Atlantic Anomaly. Proc. Natl. Acad. Sci. 119, e2200749119.
Nowaczyk, N.R., Jiabo, L., Lamy, F., Lembke-Jene, L., Arz, H.W., 2025. The Mono Lake and Laschamps geomagnetic excursions recorded by sediments in the Drake Passage. J. Geophys. Res. Solid Earth 130, e2024JB029835.
Olson, P., Amit, H., 2006. Changes in earths dipole. Naturwissenschaften 93, 519–542.
Panovska, S., Constable, C., 2017. An activity index for geomagnetic paleosecular variation, excursions, and reversals. Geochem. Geophys. Geosyst. 18, 1366–1375.
Panovska, S., Constable, C., Brown, M., 2018a. Global and regional assessments of paleosecular variation activity over the past 100 ka. Geochem. Geophys. Geosyst. 19, 1559–1580.
Panovska, S., Constable, C., Korte, M., 2018b. Extending global continuous geomagnetic field reconstructions on timescales beyond human civilization. Geochem. Geophys. Geosyst. 19, 4757–4772.
Pavón-Carrasco, F.J., Osete, M.L., Torta, J.M., De Santis, A., 2014. A geomagnetic field model for the Holocene based on archaeomagnetic and lava flow data. Earth Planet. Sci. Lett. 388, 98–109.
Sabaka, T.J., Tøffner-Clausen, L., Olsen, N., Finlay, C.C., 2020. CM6: a comprehensive geomagnetic field model derived from both CHAMP and Swarm satellite observations. Earth Planets Space 72, 80.
Sanchez, S., Fournier, A., Aubert, J., Cosme, E., Gallet, Y., 2016. Modelling the archaeomagnetic field under spatial constraints from dynamo simulations: a resolution analysis. Geophys. J. Int. 207 (2), 983–1002.
Schanner, M., Korte, M., Holschneider, M., 2022. ArchKalmag14k: a Kalman-filter based global geomagnetic model for the Holocene. J. Geophys. Res. Solid Earth 127, e2021JB023166.
Stacey, F.D., Davis, P.M., 2008. Physics of the Earth. Cambridge University Press.
Tanaka, S., Hamaguchi, H., 1997. Degree one heterogeneity and hemispherical variation of anisotropy in the inner core from PKP (BC)–PKP (DF) times. J. Geophys. Res. Solid Earth 102, 2925–2938.
Tauxe, L., 2010. Essentials of Paleomagnetism. Univ of California Press.
Terra-Nova, F., Amit, H., 2020. Magnetic boundary layers in numerical dynamos with heterogeneous outer boundary heat flux. Phys. Earth Planet. Inter. 309, 106589.
Tsang, Y.K., Jones, C.A., 2024. Scaling of the geomagnetic secular variation timescale. Geophys. J. Int. 239, 1–16.